Journal of Applied Polymer Science

# Thermo-rheological and interfacial properties of polylactic acid/polyethylene glycol blends toward the melt electrospinning ability

**Tayebe Nazari, Hamid Garmabi**
Department of Polymer Engineering and Color Technology, Amirkabir University of Technology, Tehran, 15875-4413, Iran
Correspondence to: H. Garmabi (E-mail: garmabi@aut.ac.ir)

**ABSTRACT:** The electrospinning ability of PLA/PEG system at the melt state was investigated through the viscoelastic parameters obtained from dynamic shear and extensional rheometers. PLA and PEG were melt-blended at various composition ratios. Effect of PEG concentration on the PLA thermal behavior was studied by the differential scanning calorimetry (DSC). According to DSC and wide-angle X-ray diffraction, the PLA crystallinity increased and the crystalline structure became more completed (α-crystal form) in the presence of PEG. Viscoelastic parameters such as zero-shear viscosity and relaxation time as an indication of elasticity were obtained. The results revealed enhanced polymer chain mobility and disentanglement ought to plasticizing effect of PEG. The critical content of PEG about 20–30 wt % at which the solid–liquid phase separation occurred was in good agreement with the viscoelastic properties. Hence, more than 20% PEG the elasticity diminished and the melt strength became zero. The interfacial tension of the PLA and PEG estimated through the rheological and morphological parameters evidenced the good miscibility of PLA/PEG system at the melt electrospinnig temperature. While the high viscose samples ($\eta_0 > 1800$ Pa/s) PLA and PLA/PEG (95/5) were not spinnable at the spinning temperature of 180 °C, blends containing 10–30% PEG were easily spun. The finest and continuous fiber mats were obtained by electrospinning of PLA/PEG (80/20) blend ($d_f = 4.8 \pm 0.8$ μm). More than the critical concentration of PEG ($\Phi > 30\%$), lacking the elasticity suppressed the melt electro-spinnability of PLA/PEG. © 2016 Wiley Periodicals, Inc. J. Appl. Polym. Sci. **2016**, *133*, 44120.

**KEYWORDS:** biopolymers; crystallization; electrospinning; fibers; renewable polymers; viscosity; viscoelasticity

Received 22 February 2016; accepted 23 June 2016
**DOI: 10.1002/app.44120**

## INTRODUCTION

Among the biocompatible aliphatic polyesters, polylactic acid (PLA) is one of the most promising thermoplastic finding applications going from drug-carriers and implants to packaging and textiles. High molecular weight PLA for the industrial applications is generally prepared by ring-opening polymerization of lactide as a cyclic dimer obtained from renewable sugar-based materials such as starch or cellulose.[1] Because of the chiral nature of lactic acid monomer, there are three stereoisomeric types of PLA as PLLA, PDLA, which are both semicrystalline with the same physiochemical properties, and P(D,L)LA as the commercially available PLA grade. The high melting temperature and superior processability compared with other biopolymers caused PLA to be easily processed through extrusion and cast through injection, film-blowing, thermoforming, and fiber spinning.[2] However, like other polyesters, some drawbacks including mechanical brittleness, low crystallization rate, hydrophobicity, and high cost, restrict the PLA practical uses. In addition, involvement of D- and L-units in the sequences of PLLA and PDLA during the polymerization deteriorates the thermal and mechanical properties, too. For example, 1% D-unit content in the PLLA leads to approximately 5 °C reduction in melting temperature, and about 45% increment in the crystallization half-time.[3] In order to compensate the PLA deficiencies, blending with a second polymer and/or a low molecular weight plasticizer is a convenient and economic method.[2] With this respect, researches have succeeded in the modification of PLA via blending with polyethylene glycol (PEG) with different molecular weight ranges from 200 to 200,000 g/mol.[2–15]

PEG as a hydrophilic, semi-crystalline biodegradable polymer with excellent solubility in both aqueous and organic media, belongs to the family of polyethers.[16] Biological non-toxic behavior of PEG introduces it as a reference polymer for a wide range of biomedical, biotechnological, and pharmaceutical applications. As an effective plasticizer for PLA, PEG modifies the toughness, chain mobility, crystallization rate, hydrophobicity, cell affinity, and degradation rate of PLA, insures both consumer and biomedical applications.[4,6,8–14] Adding small amount of PEG develops the shish-kebab crystalline structure of PLA under the intense shear flow filed,[17] enhances the stereocomplex crystallization of PLLA/PDLA,[18,19] homocrystallization rate of PLLA/PDLA blend under a high cooling rate,[20] aids the

transcrystallization of PLLA on the natural fiber surfaces,[21] etc. However, the amelioration of PLA properties requires the miscibility with PEG.

To date, some studies were conducted on the phase behavior of PLA/PEG blends. Younes and Cohn reported that PLA/PEG blends, representing one glass transition temperature ($T_g$), are miscible at the amorphous/melt state.[22] The enhanced crystallization of PEG components through increasing the PEG chain length and concentration was considered as a driving force for microphase segregation at the solid state. Thus, observing the ring spherulite crystalline structure of PLA film with promoted spherulite growth rate and reduced nucleation density by blending with PEG,[6,23] or interphase diffusion of PEG from PEG–PLA layer-by-layer film[24] were assessed due to partial miscibility of two components. Others tried to examine PLA/PEG miscibility thermodynamically through depression of equilibrium melting point and found a negative Flory–Huggins interaction parameter.[25] Hu *et al.*[5,26,27] studied the effect of aging at ambient temperature on glass transition ($T_g$) and obtained an Upper critical solution temperature (UCST) type phase behavior at solid state. Contemplating the solid–liquid phase separation for PLA/PEG blend, they did not investigate the blend properties after aging at temperatures higher than the melting points of PEG or PLA, unfortunately. Although the closeness of solubility parameters of PLA and PEG, 10.1 and 9.9, respectively, indicate good compatibly,[28] the large dynamic asymmetry between PLA and PEG (big difference in $T_g$) may proceed the phase immiscibility. In this line, Xu *et al.*[29] introduced the liquid-liquid phase separation (LLPS) for PLA/PEG with upper critical temperature of 160–165 °C and PEG critical concentration of 30 wt %.

Recently, melt electrospinning process have has gained considerable attentions as an eco-friendly micro/nanofiber spinning.[30–32] It has been opening the doors for three-dimensional (3D) direct writing of biopolymers in tissue engineering.[33–35] Due to high viscosity, low surface charge density and fast solidification, nano-sized fibers could be hardly obtained through the electrospinning of the melt. However, residual solvent embedded in the fiber mats menaces the cell-viability in the solvent-based electrospun scaffolds.[36] Thus, melt electrospinning can be a versatile method for the fiber spinning of PLA as a more considerable biopolymer which dissolves in toxic solvents.

Extensibility of polymer melts for fiber spinning can be assessed with the Rheotens test which is widely used in industry.[37–40] In the Rheotens, melt strength of the extruded strand is measured under the action of a tensile force and extensional deformation. Being a nonhomogeneous and nonisothermal stretching process, Rheotens resembles the actual melt spinning process. Extensional behavior is a sensitive indicator of properties concerning the molecular structure such as polydispersity, long-chain branching, and entanglement density.[40]

Performance of polymer solution or melt in the electrospinning process is closely related to the viscoelasticity of the material. However, to the best of our knowledge, this issue has not yet been studied in the melt electrospinning comprehensively. Here, attempts were made to provide deep insight into the relationships between the linear/nonlinear viscoelastic characteristics and the spinning ability of PLA/PEG blend system. In line with this, the crystallization, shear rheology and melt strength of the PLA/PEG blends, prepared by melt mixing with various blending ratios, were studied. The critical content of PEG for the solid–liquid phase separation and viscoelastisity dilution were estimated. Besides, the interfacial interaction of PLA and PEG components was evaluated through the linear dynamic rheological measurements and relaxation time of interface. Then, the blends were melt electrospun with the objective of relating the PEG content on the fiber morphology and melt electrospinnability.

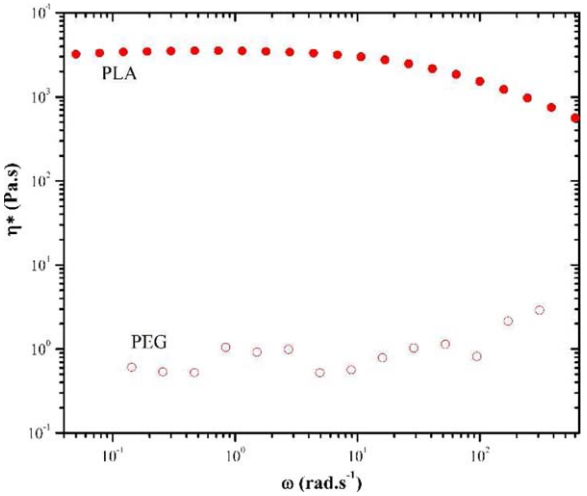


**Figure 1.** Complex viscosity versus frequency for neat PLA and PEG at 180 °C. [Color figure can be viewed in the online issue, which is available at wileyonlinelibrary.com.]

## EXPERIMENTAL

### Materials

The polylactic acid (PLA) (6350D), as an amorphous thermoplastic spunbond-grade, was obtained from NatureWorks LLC with a molecular weight at around $M_n = 116{,}000$ g/mol and polydispersity of 1.9. Polyethylene glycol (PEG), molecular weight approximately 6000 g/mol, was purchased from Kimiagaran Emrooz Co. of Iran. Figure 1 exhibited the viscosity difference of the ingredients. Irganox 1010 (Ciba Specialty Chemicals Inc., Basel, Switzerland) was applied to thermally stabilize the prepared samples.

### Preparation

PLA granules were dried in oven at the temperature of 50 °C overnight prior to compounding. PLA and PEG with composition ratios of 100/0, 95/5, 90/10, 80/20, 70/30, 50/50, and 30/70 wt/wt were melt blended in a 50 cc batch counter rotating mixer (Brabender PL2200, Germany) at 160 °C, rotor speed of 60 rpm. Since the shear effects in the batch mixer dwindled by adding highly viscose, low molecular weight PEG portion during the mixing, PLA and 0.03 wt % Irganox 1010 were firstly fed into the mixing chamber. After observation of PLA melting, PEG was fed and mixing continued for 7 min.

### Characterization

Differential scanning calorimetry (DSC) was performed with a Mettler-Toledo DSC1 calorimeter in order to evaluate the non-isothermal behavior of crystalline/crystalline polymer blends of PLA/PEG. About 4–7 mg of samples were placed into a sealed 40 μL aluminum pan and heated up to 180 °C at heating rate of 20 °C/min and kept at that temperature for 2 min to erase any thermal history. Then, cooled to 0 °C at 10 °C/min and heated up again to 180 °C (10 °C/min) under the nitrogen gas purge with a flux of 80 mL/min. Crystallinity percentage (% $X_c$) was calculated using heats of fusion of 197.7 and 93.6 J/g for PEG[41] and PLA[27] 100% crystals, respectively. Thermal properties of the samples after the melt electrospinning were also obtained during a heating scan at the rate of 10 °C/min.

The crystalline structures of samples were probed by the Wide-angle X-ray diffractometer of EQuniox 3000, Intel, with the Cu $K_\alpha$ radiation ($\lambda = 0.15418$ nm). Data were obtained at step size of 0.032°, $2\theta = 5°–80°$, and a scanning speed of 0.1°/s at room temperature.

Rheological measurements were performed using a parallel plate Paar- Physica rheometer (MCR 301, diameter of 25 mm). The gap size was adjusted at approximately 800 μm for all trails. Sample sheets for the rheological measurement were obtained by compression molding of the prepared blends into about 1 mm thick sheets at 150 °C for 3 min to avoid any thermo-oxidative degradation. Isothermal dynamic frequency sweep experiments in the range of 0.1–600 rad/s were carried out under the strain amplitude of 1%, falling well within the linear viscoelastic region, and temperature of 180 °C.

The bulk morphology of blends was observed by a Philips XL30 scanning electron microscopy (SEM) after being cryo-fractured and coated with gold. To remove the PEG domains, samples were etched by ethanol and washed with water. The number-averaged ($R_n$) and volume-averaged radii ($R_v$) of domains was determined according to the following relations:

$$R_n = \sum_i n_i R_i / \sum_i n_i \quad (1)$$

$$R_v = \sum_i n_i R_i^4 / \sum_i n_i R_i^3 \quad (2)$$

where $n_i$ is the number of the dispersed domains with radii $R_i$ counted from the SEM images.

The stretching of PLA and PLA/PEG melts were performed with a Göttfert Rheotens 71.97 melt strength tester combined with a capillary rheometer (Rheograph 6000). A die geometry ($L/D$) of 30/2 (dimensions in mm) and the die temperature of 160 °C was used for all experiments. The polymer melt strand was taken up by two wheels counter-rotating at a continuously increasing speed with the acceleration of 12 mm/s$^2$. The tensile force experienced by the strand during stretching was obtained as a function of velocity of the rollers. The force and velocity, at which the polymer melts break, are defined as the "melt strength" and "drawability," respectively. At least three replicates for each formulation were undertaken to ensure repeatability.

For the melt electrospinning experiments, a custom-designed apparatus was used (Scheme 1) which is described elsewhere in detail.[42] Granulated sample were dried in oven at the temperature of 50 °C and about 5 g of them fed into the barrel. After melting and equilibrating for at least 3 min at the spinning temperature ($T_s = 180$ °C) and flow rate of 0.5 cc/h, the high voltage power supply was turned on. The applied voltage and nozzle to collector distance set at 40 kV and 10 cm, correspondingly. The fibers were collected on an aluminum plate throughout 5 min and investigated structurally with FESEM (Mira 3-XMU, TESCAN).

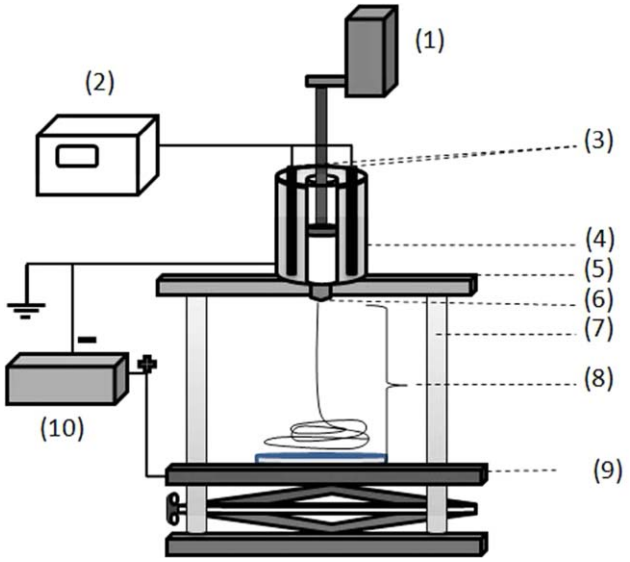


**Scheme 1.** Melt electrospinning setup. (1) syringe pump; (2) temperature controller; (3) electric heating elements; (4) metallic barrel (ID = 1 cm); (5) ceramic plate; (6) nozzle (ID = 0.2 mm); (7) wooden columns; (8) adjustable distance (1–6 cm); (9) metallic collector; (10) high voltage supply max. +75 kV. [Color figure can be viewed in the online issue, which is available at wileyonlinelibrary.com.]

## RESULTS AND DISCUSSION

### Thermal and Crystallization Behavior

Differential scanning calorimetry (DSC) is a crucial method to study melting and crystallization behavior of a polymer blend which both constituent are semi-crystalline like PLA/PEG. The thermal transitions of PLA/PEG blends during the cooling and second heating scans as DSC thermograms are shown in Figure 2. The important thermal characteristic data are summarized in Table I. The neat PLA displayed a $T_g$ at 59 °C, an slight exothermic peak of melt-recrystallization at 127 °C and an endothermic melting peak centered at 148.6 °C at the second heating process. At 5 wt % PEG concentration, the $T_g$ decreased considerably to 45 °C. The 90/10 and 80/20 blends showed the broaden glass transitions centered at 38.7 and 16 °C, respectively. Lowering the $T_g$ values is attributed to the increasing of PLA chain segmental mobility in the presence of short length PEG chains which is known as an effective plasticizer for PLA.[3] For blend compositions higher than 30 wt % concentration of PEG, the $T_g$ could not be observed by this DSC method.

According to Figure 2(a), no discernible crystallization peak of PLA and PEG was observed upon cooling up to 20% PEG content. At the 30, 50 and 70% PEG, obvious crystallization of

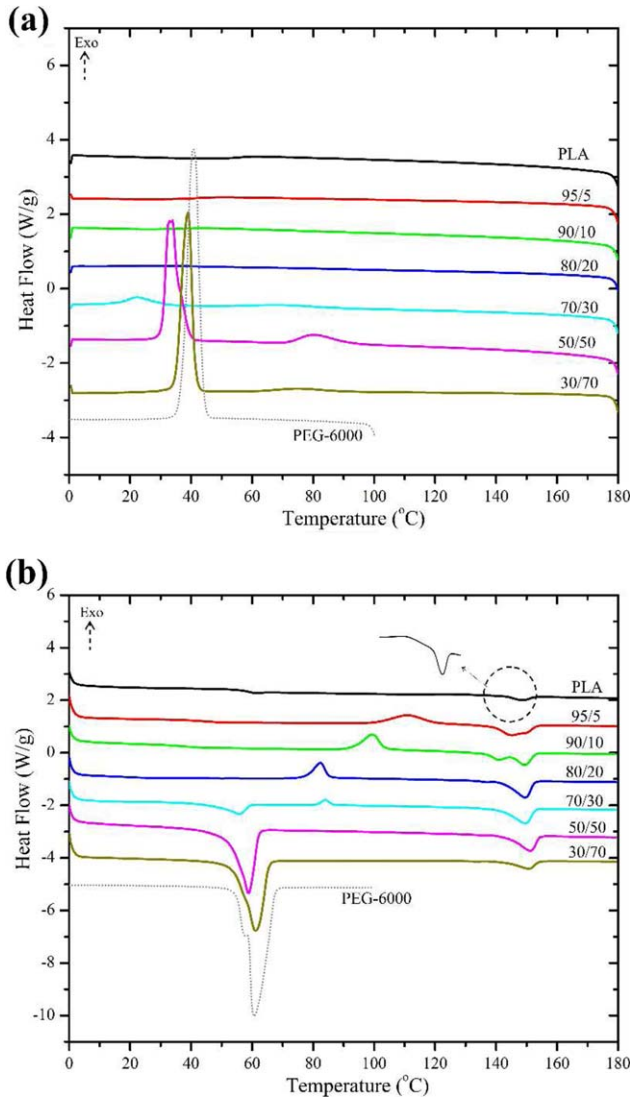


**Figure 2.** DSC thermograms recorded during (a) cooling and (b) second heating at the rate of 10 °C/min for PLA, PEG, and PLA/PEG Blends. Thermograms are shifted along vertical axis. [Color figure can be viewed in the online issue, which is available at wileyonlinelibrary.com.]

PEG and PLA phases happened at $T_c \sim 22$–40 °C and 70–80 °C, respectively. At 50/50 composition, the crystalline peak of PLA is strongest which can be attributed to the morphological effects. By increasing the PEG or decreasing the PLA content, $T_c$ of PEG increased. Actually, the microstructure of 70/30 and 50/50 blend are matrix-droplet [see Figure 7] and co-continuous (not shown here), respectively. At the amorphous region (inter-lamellar, inter-spherulitic) or melt state, PLA and PEG are miscible. During the formation of PLA crystals some molecules of PEG could be trapped in the intra-spherulitic region of PLA and led to hindering the crystallization of both PLA and PEG in 70/30 blend and decreasing the $T_c$. When the PEG domains are interconnected, PEG chains easily find a way to go out of the PLA crystalline domains. Therefore, the crystallization capacity of PLA and PEG at 50/50 blend was improved.[43,44]

Observing the separate crystallization or melting peak, Figure 2(b), for PEG domains indicated that the phase segregation of PEG occurred.[5,25] Sheth *et al.*[6] and Lai *et al.*[25] have reported the solid-liquid phase separation emanated from crystallization of PEG domains at 30 wt %. According to literature, phase separation of PEG domains may happen at lower concentration of about 10–15% by increasing the PEG molecular weight ($M_w$).[22,43–45]

At subsequent heating, cold crystallization temperature ($T_{cc}$) and enthalpy ($\Delta H_{cc}$) of PLA were monotonically depressed up to 30 wt % of PEG content and finally disappeared at 50/50 and 30/70 blends. Incomplete crystallization of PLA at cooling stage would cause cold crystallization due to rearrangement of polymer chains at heating stage before melting.[4,9–12,14,46] Increasing the amount of PEG shifted $T_{cc}$ and $T_g$ to lower temperature owing to facilitating of the chain ability for rearrangement. This leads to easily crystallization and increasing the crystallinity percentage ($X_c$) of PLA. Enhancing the crystallinity or decreasing the amount of the amorphous phase could be inferred from broadening of the glass transition for the crystallized plasticized PLA, too.[4] However, at 5 wt % PEG, the cold crystallization enthalpy ($\Delta H_{cc}$), 25 J/g, was very close to the melting enthalpy ($\Delta H_m = 25.7$ J/g), evidencing that the sample was amorphous ($X_{cPLA} = 0.7\%$). Therefore, improving the chain

**Table I.** Results from DSC for the PLA/PEG Blends at Scan Rate of 10 °C/min

| | PEG phase | | | | PLA phase | | | | | | |
|---|---|---|---|---|---|---|---|---|---|---|---|
| Sample | $T_c$ (°C) | $T_m$ (°C) | $\Delta H_m$ (J/g) | $X_c$ (%) | $T_g$ (°C) | $T_{cc}$ (°C) | $T_c$ (°C) | $T_m$ (°C) | $\Delta H_{cc}$ (J/g) | $\Delta H_m$ (J/g) | $X_c$ (%) |
| PLA | — | — | — | — | 59 | — | — | 148.6 | 2.6 | 5.2 | 2.8 |
| 95/5 | — | — | — | — | 45 | 111 | — | 144.6, 149.2 | 25 | 25.7 | 0.7 |
| 90/10 | — | — | — | — | 38.7 | 99.5 | — | 141, 149.5 | 25.7 | 28.9 | 9.9 |
| 80/20 | — | — | — | — | 16 | 82.3 | — | 137, 150 | 19.1 | 27.5 | 11.2 |
| 70/30 | 22.6 | 55.9 | 19.7 | 33 | — | 83.9 | 70 | 149.5 | 5.2 | 25.9 | 31.6 |
| 50/50 | 33 | 58.9 | 97.8 | 98 | — | — | 80.6 | 151 | — | 25 | 53.4 |
| 30/70 | 38.9 | 61.3 | 127.7 | 92 | — | — | 75 | 150.7 | — | 12.8 | 45.5 |
| PEG | 40.8 | 60.5 | 197.3 | 100 | — | — | — | 60.5 | — | — | — |

$X_{cPLA}$ (%) $= \frac{\Delta H_m - \Delta H_{cc}}{\Phi_{PLA} \times 93.6} \times 100$, $X_{cPEG}$ (%) $= \frac{\Delta H_m}{\Phi_{PEG} \times 197.7} \times 100$.

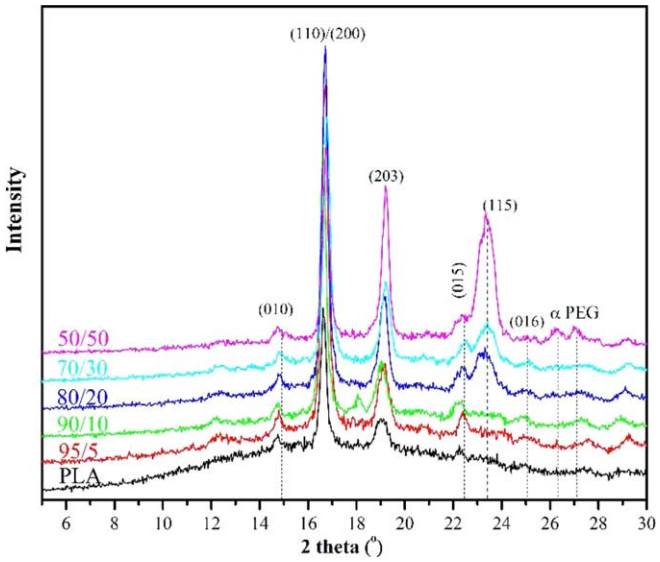


**Figure 3.** Wide-angle X-ray diffraction (WAXD) spectrograms of pure PLA and PLA/PEG blends. [Color figure can be viewed in the online issue, which is available at wileyonlinelibrary.com.]

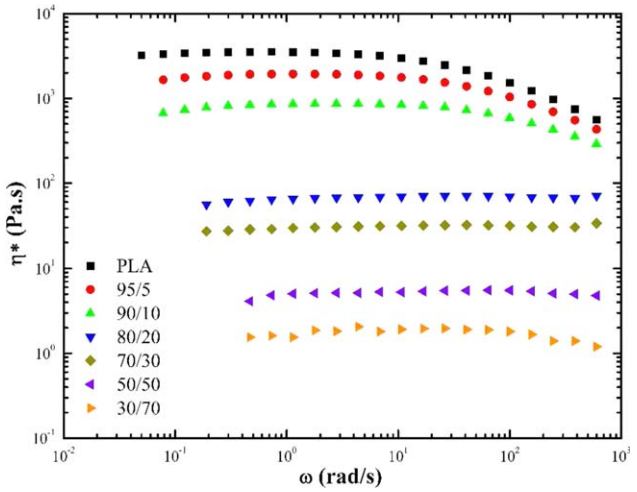


**Figure 4.** Dynamic viscosity versus frequency for PLA and PLA/PEG blends at 180 °C. [Color figure can be viewed in the online issue, which is available at wileyonlinelibrary.com.]

motion would affect the state of the crystals perfection or crystallite sizes at this content of PEG which can be discussed more through melting peaks.

On the thermogram, the neat PLA showed the one melting peak with a negligible enthalpy (5.2 J/g). In the PLA/PEG (95/5) blend broaden melting transition with two shoulder appeared at 144.6 and 149.5 °C. By adding 10 wt % PEG, more pronounced double peak with shifting the lower peak temperature to 141 °C were observed. While the other one at about 150 °C, as the main peak, was not affected. For all blends, the main melting temperature was approximately unchanged at 150 °C and the shoulder peak disappeared for higher PEG content, more than 20 wt %. Multiple melting behavior of neat PLA, PLLA and their blends with PEG at different $M_w$ (500–8000 g/mol) up to 30 wt % PEG have been reported, recently.[4,14,27,47,48]

Generally, multiple melting indicates (i) the melting of different crystalline structure (polymorphism) or thickness, and (ii) melt-recrystallization or crystal phase transition process. They result in the endotherm and exotherm in the DSC curve, correspondingly. Recently, polymorphous crystallization and multiple melting behavior of PLA depending on the crystallization temperature have been investigated.[47,48] Accordingly, α and α′ (disordered α) crystalline structures form at high ($T_c > 120$ °C) and low ($T_c < 100$ °C) crystallization temperature, respectively. Between the range of above mentioned temperatures, $T_c$ = 100–120 °C, the α and α′ crystals coexist. Difficulties for the chain mobility and diffusion at lower $T_c$'s, creates the incomplete and unstable α′ crystals. They incline to change the phase to α and become more stable with losing the excess energy. So, at the second heating scan, the slight exothermic peak joined to melting of neat PLA indicates the presence of incomplete crystalline or α′ structures.[49] Double melting peak of 95/5, 90/10, and 80/20 blends is due to coexistence of both α and α′-forms. At 30–50 wt % PEG loaded blends, PLA crystallization might be perfect.[43] Consequently, increasing the PEG content, improves the both crystallinity and crystal structures.

Figure 3 shows the WAXD spectrum of PLA/PEG samples. The typical reflections of α-form crystal at 2θ = 15.1°, 16.9°, 19.2°, and 22.5° corresponding to lattice planes (010), (200)/(110), (203), and (015), respectively, can be observed for crystalline PLA phase.[17,50] These lattice planes are shifted to lower 2θ degrees up to 20 wt % PEG, emanated from incomplete crystallization or α′ phase with lower packing density. In addition, by perfection of crystalline structure, other lattice planes of (115) and (016) appear at higher PEG loading. The X-ray diffraction pattern supports the DSC results about the presence of α′ crystal phase of PLA up to 20 wt %.

### Rheological and Interfacial Properties

To elucidate the plasticizing effect of PEG and phase morphology of PLA/PEG blends, melt rheological properties were investigated under the shear flow. Figure 4 represents the frequency dependence of dynamic viscosity at various PEG concentrations at 180 °C. Neat PLA shows a non-Newtonian behavior, a Newtonian Plateau at low oscillation frequency with the zero-shear

**Table II.** Zero-Shear Viscosity ($\eta_0$) and Relaxation Time ($\tau_0$) at 180 °C for Neat PLA and PLA/PEG Blends

| sample | PLA | 95/5 | 90/10 | 80/20 | 70/30 | 50/50 | 30/70 |
|---|---|---|---|---|---|---|---|
| $\eta_0$ (Pa s) | 3485 | 1893.2 | 857.2 | 56.6 | 29.8 | 5.4 | 2.38 |
| $\tau_0$ (s) | 0.1 | 0.07 | 0.03 | 0.06 | 0.08 | $4.5 \times 10^{-5}$ | $1.1 \times 10^{-4}$ |

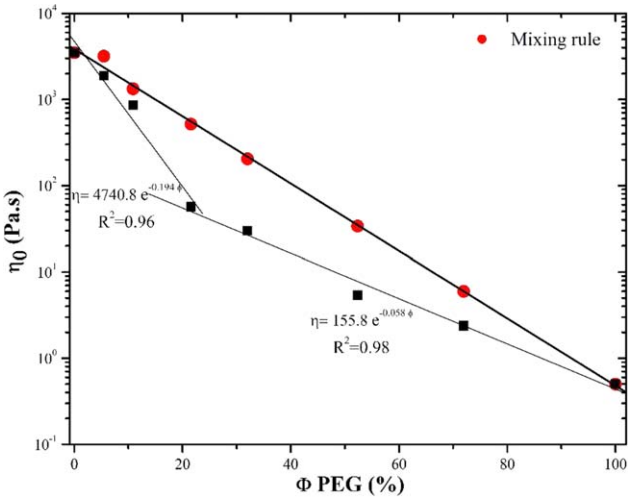


**Figure 5.** Terminal viscosity ($\eta_0$) versus volume fraction of PEG ($\Phi$), and viscosities according to mixing rule. [Color figure can be viewed in the online issue, which is available at wileyonlinelibrary.com.]

rate viscosity around 3500 Pa s and a slight shear thinning behavior at high oscillation frequency ($\sim\omega > 2$ rad/s).

By varying the PEG content in all PLA/PEG blends, a more pronounced Newtonian response with an extended Newtonian plateau compared with pure PLA is observable. Increasing the PEG concentrations causes the great viscosity reduction in the blends.[13,44,45] This could confirm the disentanglement and increasing the segmental mobility of PLA chain due to plasticizing effect of PEG.

Using the loss ($G''$) and storage modulus ($G'$) versus frequency curves, Figure 6, at terminal frequencies zero-shear viscosity ($\eta_0$) and longest relaxation time ($\tau_0$) are provided by the following relations[51]:

**Table III.** Calculated Interfacial Tension for PLA and PEG at 180 °C

| Equation | γ (mN/m) |
|---|---|
| Palierne | 0.0434 |
| G-M | 0.0956 |
| Geometric-mean | 0.79 |

$$\eta_0 = \lim_{\omega \to 0} \frac{G''}{\omega} \tag{3}$$

$$\tau_0 = \lim_{\omega \to 0} \frac{G'}{G''\omega} \tag{4}$$

The obtained values are summarized in Table II. The semi-log graph of $\eta_0$ versus volume fraction of PEG ($\Phi$) and the calculated viscosity according to the mixing rule, given in the following form:

$$\log \eta = \varphi \log \eta_{PEG} + (1-\varphi)\log \eta_{PLA} \tag{5}$$

are plotted at Figure 5. The slope of $\eta_0 - \varphi$ up to 20% PEG ($\ln\eta \sim -0.194\varphi$) is different from the 30 to 100% PEG ($\ln\eta \sim -0.058\varphi$) confirming the plasticizer saturation point could be reached at $\phi_c \sim$ 20–30%.[9] Reminiscing the separate crystallization/melting behavior of PEG domains at the concentration range more than 20% (Figure 2), this rheological observations verify the critical content of PEG obtained by DSC. On the other hand, all PLA/PEG blends display a negative deviation from the mixing rule. However, they are at the homogenous state.[29] Decreasing the viscosity of a polymer blend at the phase miscible state and also, the negative divergence of the low molecular weight ones without the chain entanglement have been reported by Vlassopoulos *et al.*[52,53] Since the molecular weight of PEG chains are around the average molecular weight between entanglements for polymer chains, $M_e \sim$ 6000 g/mol,

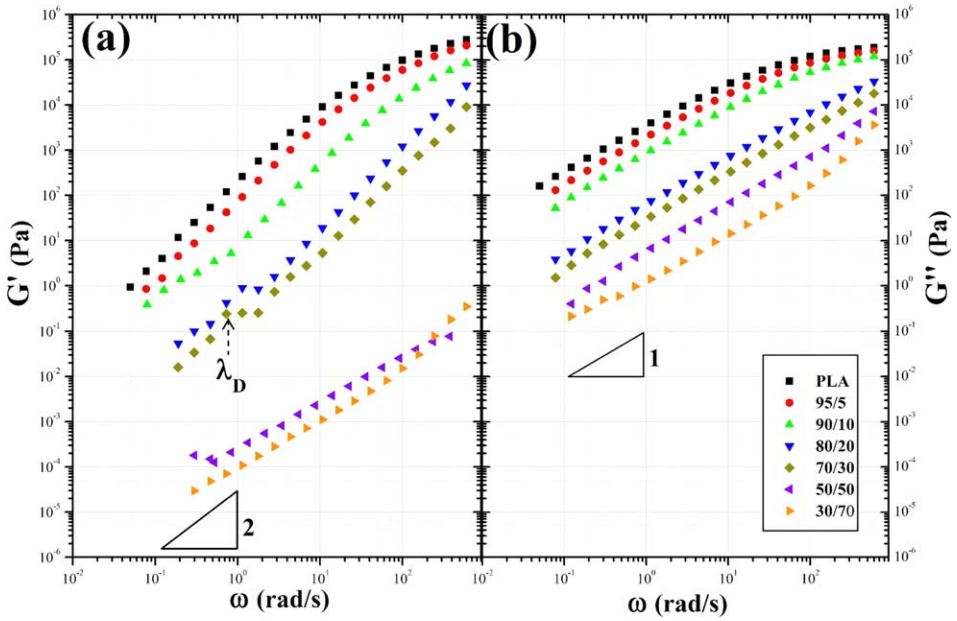


**Figure 6.** (a) Storage ($G'$) and (b) loss modulus ($G''$) versus frequency for PLA and PLA/PEG blends at 180 °C. [Color figure can be viewed in the online issue, which is available at wileyonlinelibrary.com.]

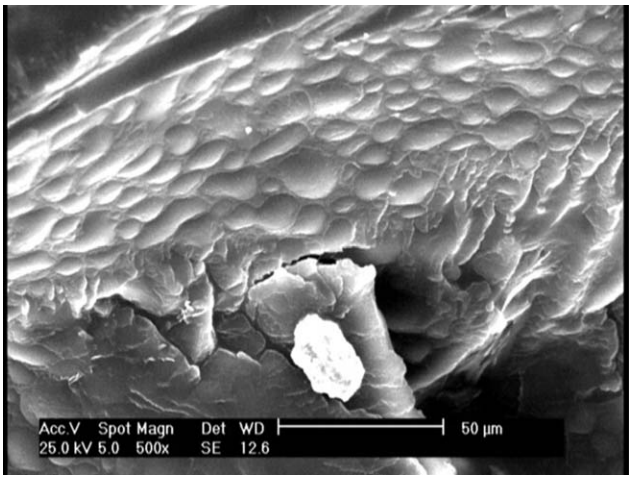


**Figure 7.** SEM image from the bulk morphology of 70/30 blend at 180 °C.

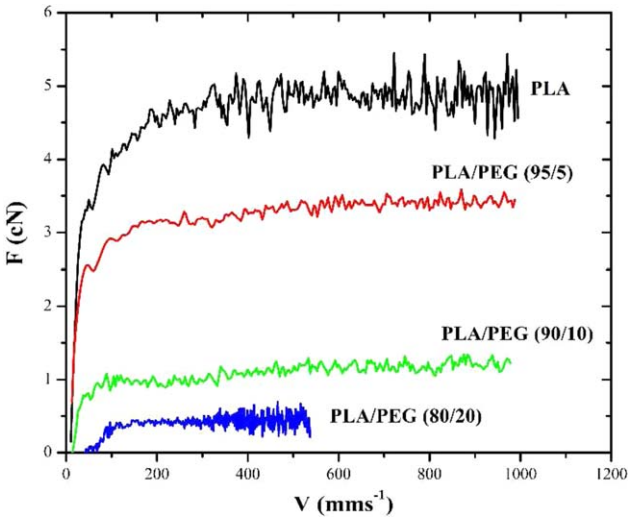


**Figure 8.** Rheotens force curves for PLA and its blends with PEG. [Color figure can be viewed in the online issue, which is available at wileyonlinelibrary.com.]

they are disentangled. Having the good thermodynamically interaction with PLA chains, raising the PEG amount extremely reduces the entanglement density. Therefore, increasing the free volume between the PLA chains brings about the abrupt reduction in $\eta_0$ and negative deviation from the mixing rule.

Figure 6(a,b) demonstrate the corresponding storage and loss modulus of PLA/PEG blends. As expected, the dynamic modulus of PLA decreased with increasing the plasticizer loading at all frequencies. The pronounced, three order of magnitude reductions of the storage modulus and in-range decrements of loss modulus for 50/50 and 30/70 blends emphasis the more viscose-like behavior of low molecular weight PEG ingredient. Moreover, the values of relaxation time for these blends are near zero ($\tau_0 \leq 10^{-4}$) according to Table II, confirming Newtonian behavior. A typical scaling laws of $G' \sim \omega^2$ and $G'' \sim \omega$ at low frequencies in the terminal region for a well-homogeneous polymer blend are obtained up to 30% PEG. While for 50/50 and 30/70 blend, the terminal slope of both $G'$ and $G''$ is about 1. For these two blends the structure might be co-continuous, phase-inverted or inhomogeneous.[45]

At low frequencies, $G'(\omega)$ of blends exhibited a relaxation shoulder which moved toward medium frequencies at 20 and 30% PEG and became more pronounced. This behavior is attributed to the shape relaxation of ellipsoidal deformed droplets back to spheres.[54–56] It is considered as a typical linear viscoelastic performance of a dilute polymer blends with the matrix-dispersed morphology which is certified from SEM analysis of sample 70/30 after cryo-fracturing and etching the PEG droplets, Figure 7. At Terminal zone, the modulus of a mixture is dominated by the dynamics of interface which is depended on interfacial tension and droplet shape deformation.[57] Using some theoretical emulsion models like Palierne[58] and Gramespacher and Meissner (G–M),[59] it is possible to calculate the interfacial tension ($\lambda$). According to Palierne, when the dispersion of droplet sizes are narrow, $R_v/R_n \leq 2.3$, the longest relaxation time ($\lambda_D$) can be calculated as follows:

$$\lambda_D = \frac{R\eta_m}{4\gamma}\frac{(19k+16)[2k+3-2\varphi(k-1)]}{10(k+1)-2\varphi(5k+2)} \quad (6)$$

where $\eta_m$ is the matrix viscosity, $k$, the zero-shear viscosity ratio of dispersed to matrix ($\eta_d/\eta_m$), and $\varphi$, the volume fraction of the dispersed component. Knowing the droplet radius and relaxation time of interface $\lambda_D$ [shown in Figure 6(a)], it's possible to estimate the interfacial tension through rheological parameters.

Also, according to G–M model, interface relaxation can be estimated as following equation:

$$\lambda_D = \left(\frac{R\eta_m}{\gamma}\right)\frac{(19k+16)(2k+3)}{40(k+1)}\left\{1+\varphi\left[\frac{5(19k+16)}{4(k+1)(2k+3)}\right]\right\} \quad (7)$$

For 70/30 PLA/PEG sample with the average $R_v$ and $R_n$ about 5.6 µm and 4.69 µm ($R_v/R_n$=1.2), respectively, the characteristic relaxation time is $\lambda = {}^{1}/_{\omega(0.732)} = 1.36$ s from Figure 6(a). Applying the $\eta_m$ = 3485 Pa.s, and $\eta_d$ = 0.5 Pa s, interfacial tension was calculated from eqs. (6) and (7) at 180 °C, summarized at Table III. To verify the obtained value, interfacial tension ($\gamma_{12}$) can be estimated through the geometric-mean equation, too:

**Table IV.** Melt Strength ($F$), Drawability ($V$), and Melt Electrospun Fiber Diameter ($d_f$) for PLA and PLA/PEG Blends

| Sample | PLA | 95/5 | 90/10 | 80/20 | 70/30 | 50/50 | 30/70 |
|---|---|---|---|---|---|---|---|
| $F$ (cN) | 4.75 | 3.45 | 1.22 | 0.21 | ~0 | 0 | 0 |
| $V$ (mm/s) | 994 | 988 | 978 | 537 | ~0 | 0 | 0 |
| $d_f$ (µm) | No jet | No jet | 30 ± 3 | 4.8 ± 0.8 | 5.2 ± 1 | No fiber | No fiber |

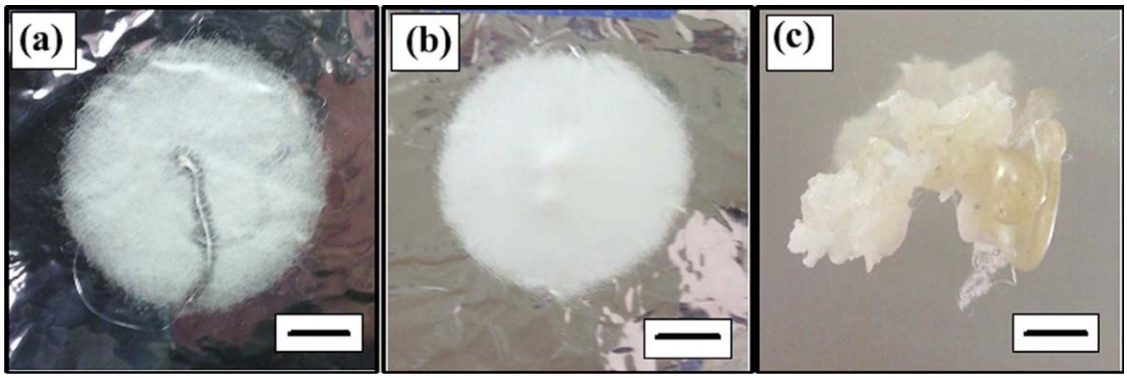


**Figure 9.** Camera image of (a) 90/10 and (b) 70/30 fiber mats, and not spinnable (c) 50/50 sample after melt electrospinning. Scale bar = 1 cm. [Color figure can be viewed in the online issue, which is available at wileyonlinelibrary.com.]

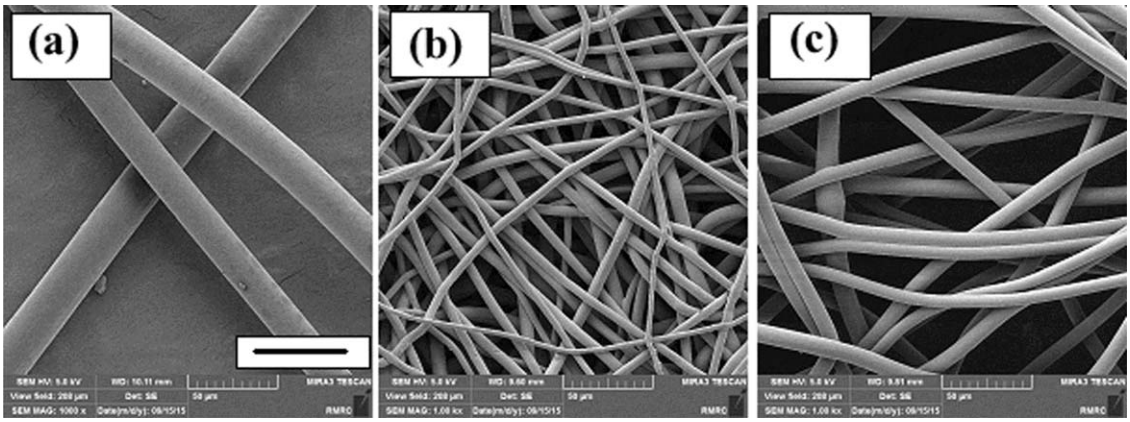


**Figure 10.** FESEM images of PLA/PEG based melt electrospun fibers (a) 90/10, (b) 80/20, and (c) 70/30. Scale bar = 50 μm.

$$\gamma_{12}=\gamma_1+\gamma_2-2\left(\sqrt{\gamma_1^d\gamma_2^d}+\sqrt{\gamma_1^p\gamma_2^p}\right) \quad (8)$$

where $\gamma_i^d$ and $\gamma_i^p$ are denoted the dispersive and polar components of surface tension $\gamma_i$ of ingredients. This equation is suitable for systems with higher surface energy more than 20 mN/m.[60] Using the literature values of surface energy for PLA ($\gamma = 40.7$ mN/m, $\gamma^d = 32.5$, and $\gamma^p = 8.2$ at 25 °C[61]) and PEG ($\gamma = 42.8$ mN/m, $\gamma^d = 12.2$, and $\gamma^p = 30.6$ at 20 °C[41]) and the common temperature coefficient of $d\gamma/dT = -0.07$ mN/m/K, interfacial tension was found to be 0.79 mN/m. This value, as the static interfacial tension of PEG with PLA ($\gamma_{12}^0$), is an order of magnitude higher than the ones estimated through the structural parameters using a dynamic techniques like rheology. Since PLA melt is a viscoelastic fluid and PEG melt is viscose, the second normal stress of PLA as the matrix phase ($N_{2,m}$) is enormously larger than PEG droplets ($N_{2,d}$). In accordance with Vanoene [eq. (9)] dynamic interfacial tension possess lower values than static one.[62]

$$\gamma_{12}=\gamma_{12}^0+\frac{D_d}{12}(N_{2.d}-N_{2.m}) \quad (9)$$

As the obtained values of $\gamma_{12}$ at Table III are near zero, the good miscibility of PLA/PEG will be confirmed.

### Spinnability through Rheotens and Melt Electrospinnig

It is clear that the polymers melt with low molecular weight, low branched chains and addition of plasticizers will have lower

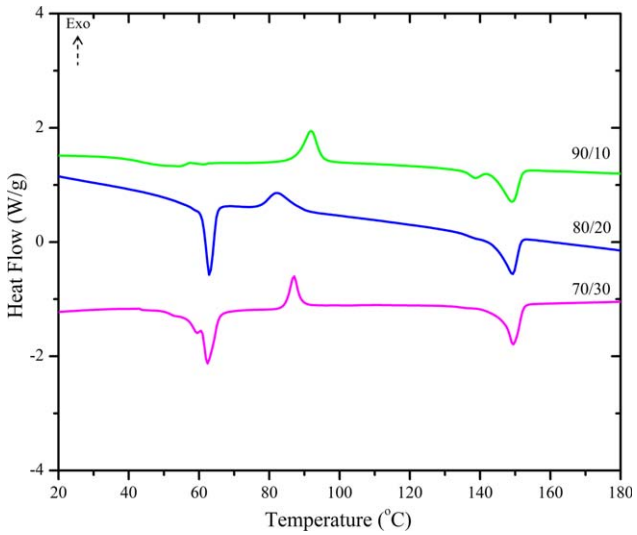


**Figure 11.** DSC thermograms recorded during first heating at the rate of 10 °C/min for electrospun PLA/PEG fibers at 90/10, 80/20, and 70/30 composition ratio. [Color figure can be viewed in the online issue, which is available at wileyonlinelibrary.com.]

**Table V.** Results from DSC for Electrospun PLA/PEG Fibers

| Sample | PEG phase | | | PLA phase | | | | | |
|---|---|---|---|---|---|---|---|---|---|
| | $T_m$ (°C) | $\Delta H_m$ (J/g) | $X_c$ (%) | $T_g$ (°C) | $T_{cc}$ (°C) | $T_m$ (°C) | $\Delta H_{cc}$ (J/g) | $\Delta H_m$ (J/g) | $X_c$ (%) |
| 90/10 | 61 | 0.4 | 2 | 42.3 | 91.8 | 138.8, 149.5 | 16.6 | 23.5 | 8.2 |
| 80/20 | 62.8 | 22.7 | 57.4 | — | 82.3 | 139,149 | 11.7 | 23.1 | 15.2 |
| 70/30 | 62.4 | 32 | 53.9 | — | 86.9 | 136, 149.5 | 10.5 | 23.9 | 20.5 |

melt elasticity.[63] Figure 8 exhibits the measured tensile force as a function of drawdown speed for PLA and PLA/PEG melts gained from Rheotens experiments. The dilution effect of PEG results in easily slippage of the PLA chains and considerable reduction of the melt strength. Meanwhile, the low viscose samples 70/30, 50/50, and 30/70 were sagging on their own weight, the melt strength is near the detection limit of the instrument (~0) or not extensible, [Table IV]. Rheotens measurements reassure again the disentanglement of PLA chains in the presence of PEG and diminishing the elastic responses of the melt in polymer blends with concentration more than critical composition $\phi_c$ (20–30 wt %).

In the melt electrospinning procedure, no jet formed from the neat PLA and 95/5 melts due to high viscosity and melt strength. They were not spinnable at 180 °C. While, the nonwoven fiber mats of 10–30% PEG loading blends were achieved successfully, Figure 9(a,b). The average fiber diameters ($d_f$) are tabulated in Table IV and the morphology depicted in Figure 10. At 50 and 70% PEG, a melt drop emerging out of the nozzle grew larger instead of the jet formation. Having no elasticity and high crystallization rate, the drop solidified very fast and fell downward without stretching, Figure 9(c). In the solution elecrospinning, lacking the elasticity gives rise to electrospraying or bead-on-string fiber morphology due to Rayleigh instability of dilute solutions.[64,65] Here for a polymer melt as a concentrated solution, sagging and no fiber mat formation arise when the elasticity is lost.

According to Figure 10, the obvious reduction of fiber diameter is achieved by increasing the PEG concentration from 10 to 30 wt %. As Rheotens melt strength of sample 70/30 was near zero, the best melt electrospinnability is found for 80/20 PLA/PEG sample with the smaller fiber diameter. As a consequence, easily spinnable PLA fibers could be prepared by incorporation of PEG as a viscosity reducing and melt electrospinnabity increasing agent. The fabricated PLA/PEG nonwoven mats have a potential application in the tissue engineering directly.

**Thermal Properties of Melt-Electrospun Fibers**

The thermal properties of electrospun PLA/PEG blend fibers during the first heating scan are shown in Figure 11 and Table V. All the fibers present cold-crystallization and double-melting behavior owing to rapid solidification and incomplete crystallization during the elctrospinning process. Fiber 90/10 shows $T_g$ at 42.3 °C, about 3.6 °C higher than the $T_g$ of bulk 90/10 sample (Table I), confirms the confinement of the amorphous phase because of drawing.[66] Comparing with the bulk samples, main melting temperature of fibers again is fixed at about 150 °C. While the critical composition of PEG for solid-liquid phase separation was at $\phi_c = 30$ wt % at the bulk state (Figure 2), separate melting endotherm for PEG phase is observable at 61–62 °C in all fibers. Also, crystallinity degree of PEG phase ($X_{c\text{-}PEG}$) is increased by melt electrospinning but of PLA ($X_{c\text{-}PLA}$) is decreased. Higher capacity of PEG chains for crystallization under the intense shear can be deduced. In other words, the tendency toward the solid-liquid phase separation of PEG in the PLA/PEG systems is raised by the melt electrospinning process.[67]

## CONCLUSIONS

In the present work, effect of PEG concentration on the viscoelasticity and spinnability of PLA/PEG system spun by a custom-built melt electrospinning setup, have been comprehensively studied. Obviously, incorporation of PEG would results in enhancing the chain segmental mobility, decreasing the viscosity, and reducing the entanglement density. Easily slippage of PLA chains demonstrated the considerable influence on the melt strength from the Rheotens. Blending with PEG presented more perfect crystalline structure for PLA. Calculated interfacial interaction using the rheological parameters and theoretical approaches, confirmed the miscibility of PLA/PEG blend system at the melt electrospinning temperature. The critical concentration of PEG phase segregation at the solid state and viscoelasticity dilution were obtained to be $20 < \phi_c < 30$ wt %. Easily melt spun PLA/PEG microfibers in the ranges of 10–30 wt % PEG with the minimum diameter of $4.8 \pm 0.8$ μm was obtained. The melt electrospinnability was not possible for neat PLA due to high viscosity, as well for the blend compositions more than $\phi_c$ due to lacking the elastic responses of the melt. Melt electrospun fibers presented lower crystallinity and segregation of PEG domains.

## ACKNOWLEDGMENTS

The authors thank Prof. V. Altstädt at Department of Polymer Engineering, Universiy of Bayreuth and special thanks to Ms. Jacqueline Uhm for running the Rheotens experiments at Rheology Lab.

## REFERENCES

1. Smith, R. Biodegradable Polymers for Industrial Applications; Woodhead Publishing Limited: Cambridge, **2005**.

2. Rasal, R. M.; Janorkar, A. V.; Hirt, D. E. *Prog. Polym. Sci.* **2010**, *35*, 338.
3. Saeidlou, S.; Huneault, M. A.; Li, H.; Park, C. B. *Prog. Polym. Sci.* **2012**, *37*, 1657.
4. Kulinski, Z.; Piorkowska, E. *Polymer* **2005**, *46*, 10290.
5. Hu, Y.; Hu, Y. S.; Topolkaraev, V.; Hiltner, A.; Baer, E. *Polymer* **2003**, *44*, 5681.
6. Sheth, M.; Kumar, R. A.; Dave, V.; Gross, R. A.; Mccarthy, S. P. *J. Appl. Polym. Sci.* **1997**, *66*, 1495.
7. Pillin, I.; Montrelay, N.; Grohens, Y. *Polymer* **2006**, *47*, 4676.
8. Baiardo, M.; Frisoni, G.; Scandola, M.; Rimelen, M.; Lips, D.; Ruffieux, K.; Wintermantel, E. *J. Appl. Polym. Sci.* **2003**, *90*, 1731.
9. Hongbo, L.; Huneault, M. A. *Polymer* **2007**, *48*, 6855.
10. Sungsanit, K.; Kao, N.; Bhattacharya, S. N.; Pivsaart, S. *Korea-Australia Rheol. J.* **2010**, *22*, 187.
11. Hassouna, F.; Raquez, J. M.; Addiego, F.; Dubois, P.; Toniazzo, V.; Ruch, D. *Eur. Polym. J.* **2011**, *47*, 2134.
12. Chieng, B. W.; Ibrahim, N. A.; Yunus, W. M. Z. W.; Hussein, M. Z. *J. Appl. Polym. Sci.* **2013**, *130*, 4576.
13. Feng, L.; Bian, X.; Chen, Z.; Li, G.; Chen, X. *Polym. Degrad. Stabil.* **2013**, *98*, 1591.
14. Yu, Y.; Cheng, Y.; Ren, J.; Cao, E.; Fu, X.; Guo, W. *J. Appl. Polym. Sci.* **2015**, *132*, DOI: 10.1002/app.41808.
15. Nijenhuis, A. J.; Colstee, E.; Grijpma, D. W.; Pennings, A. J. *Polymer* **1996**, *37*, 5849.
16. Tian, H.; Tang, Z.; Zhuang, X.; Chen, X.; Jing, X. *Prog. Polym. Sci.* **2012**, *37*, 237.
17. Xu, H.; Zhong, G. J.; Fu, Q.; Lei, J.; Jiang, W.; Hsiao, B. S.; Li, Z. M. *ACS Appl. Mater. Interfaces* **2012**, *4*, 6774.
18. Bao, R. Y.; Yang, W.; Wei, X. F.; Xie, B. H.; Yang, M. B. *ACS Sustain. Chem. Eng.* **2014**, *2*, 2301.
19. Saeidlou, S.; Huneault, M. A.; Li, H.; Park, C. B. *Polymer* **2013**, *54*, 5762.
20. Wei, X. F.; Bao, R. Y.; Cao, Z. Q.; Zhang, L. Q.; Liu, Z. Y.; Yang, W.; Xie, B. H.; Yang, M. B. *Colloid Polym. Sci.* **2014**, *292*, 163.
21. Xu, H.; Xie, L.; Jiang, X.; Li, X. J.; Li, Y.; Zhang, Z. J.; Zhong, G. J.; Li, Z. M. *J. Phys. Chem. B* **2014**, *118*, 812.
22. Younes, H.; Cohn, D. *Eur. Polym. J.* **1988**, *24*, 765.
23. Yang, J. M.; Chen, H. L.; You, J. W.; Hwang, J. C. *Polym. J.* **1997**, *29*, 657.
24. Zhang, Y.; Wang, Z.; Jiang, F.; Bai, J.; Wang, Z. *Soft Matter* **2013**, *9*, 5771.
25. Lai, W. C.; Liau, W. B.; Lin, T. T. *Polymer* **2004**, *45*, 3073.
26. Hu, Y.; Rogunova, M.; Topolkaraev, V.; Hiltner, A.; Baer, E. *Polymer* **2003**, *44*, 5701.
27. Hu, Y.; Hu, Y. S.; Topolkaraev, V.; Hiltner, A.; Baer, E. *Polymer* **2003**, *44*, 5711.
28. Montero, N. H.; Ugartemendia, J. M.; Amestoy, H.; Sarasua, J. R. *J. Polym. Sci. Part B: Polym. Phys.* **2014**, *52*, 111.
29. Xu, Y.; Yu, W.; Zhou, C. *RSC Adv.* **2014**, *4*, 55435.
30. Góra, A.; Sahay, R.; Thavasi, V.; Ramakrishna, S. *Polym. Rev.* **2011**, *51*, 265.
31. Shimada, N.; Ogata, N.; Nakane, K.; Ogihara, T. *J. Appl. Polym. Sci.* **2012**, *125*, 384.
32. Zhmayev, E.; Cho, D.; Joo, Y. L. *Polymer* **2010**, *51*, 4140.
33. Hochleitner, G.; Hümmer, J. F.; Luxenhofer, R.; Groll, J. *Polymer* **2014**, *55*, 5017.
34. Ristovski, N.; Bock, N.; Liao, S.; Powell, S. K.; Ren, J.; Kirby, G. T. S.; Blackwood, K. A.; Woodruff, M. A. *Biointerphases* **2015**, *10*, 011006.
35. Bas, O.; De-Juan-Pardo, E. M.; Chhaya, M. P.; Wunner, F. M.; Jeon, J. E.; Klein, T. J.; Hutmacher, D. W. *Eur. Polym. J.* **2015**, *72*, 451.
36. Lee, H.; Ahn, S.; Choi, H.; Cho, D.; Kim, G. H. *J. Mater. Chem. B* **2013**, *1*, 3670.
37. Wagner, M. H.; Schulze, V.; Gottfert, A. *Polym. Eng. Sci.* **1996**, *39*, 925.
38. Laun, H. M.; Schuch, H. *J. Rheol.* **1989**, *33*, 119.
39. Baldi, F.; Franceschini, A.; Riccò, T. *Rheol. Acta* **2007**, *46*, 965.
40. Doufas, A. K.; Rice, L.; Thurston, W. *J. Rheol.* **2011**, *55*, 95.
41. Mark, J. E. Polymer Data Handbook; Oxford University Press: Oxford, **1999**.
42. Nazari, T.; Garmabi, H. *Micro Nano Lett.* **2014**, *9*, 686.
43. Li, F. J.; Zhang, S. D.; Liang, J. Z.; Wang, J. Z. *Polym. Adv. Technol.* **2015**, 26.
44. Sungsanit, K.; Kao, N.; Bhattacharya, S. N. *Polym. Eng. Sci.* **2012**, *52*, 108.
45. Li, F. J.; Tan, L. C.; Zhang, S. D.; Zhu, B. *J. Appl. Polym. Sci.* **2016**, *133*, DOI: 10.1002/app.42920.
46. Ren, Z.; Dong, L.; Yang, Y. *J. Appl. Polym. Sci.* **2006**, *101*, 1583.
47. Zhang, J.; Tashiro, K.; Tsuji, H.; Domb, A. J. *Macromolecules* **2008**, *41*, 1352.
48. Pan, P.; Kai, W.; Zhu, B.; Dong, T.; Inoue, Y. *Macromolecules* **2007**, *40*, 6898.
49. Kalish, J. P.; Aou, K.; Yang, X.; Hsu, S. *Polymer* **2011**, *52*, 814.
50. You, J.; Yu, W.; Zhou, C. *Ind. Eng. Chem. Res.* **2014**, *53*, 1097.
51. Macosko, C. W. Rheology: Principles, Measurements, and Applications; VCH: New York, **1993**.
52. Kapnistos, M.; Hinrichs, A.; Vlassopoulos, D.; Anastasiadis, S. H.; Stammer, A.; Wolf, B. A. *Macromolecules* **1996**, *29*, 7155.
53. Vlassopoulos, D.; Koumoutsakos, A.; Anastasiadis, S. H.; Hatzikiriakos, S. G.; Englezos, P. *J. Rheol.* **1997**, *41*, 739.
54. Graebling, D.; Muller, R.; Palierne, J. F. *Macromolecules* **1993**, *26*, 320.
55. Pötschke, P.; Paul, D. R. *J. Macromol. Sci. Part C: Polym. Rev.* **2003**, *C43*, 87.
56. Bousmina, M. *Rheol. Acta* **1999**, *38*, 251.

57. Yeganeh, J. K.; Goharpey, F.; Foudazi, R. *Macromolecules* **2010**, *43*, 8670.

58. Palierne, J. F. *Rheol. Acta* **1990**, *29*, 204.

59. Gramespacher, H.; Meissner, J. *J. Rheol.* **1992**, *36*, 1127.

60. Wu, S. Polymer Interface & Adhesion; Marcel Dekker: New York, **1982**.

61. Khoshkava, V.; Kamal, M. R. *Biomacromolecules* **2013**, *14*, 3155.

62. Vanoene, H. *J. Colloid. Interface Sci.* **1972**, *40*, 448.

63. Sears, J. K.; Darby, J. R. Technology of Plasticizers; John Wiley & Sons: New York, **1982**.

64. Yu, J. H.; Fridrikh, S. V.; Rutledge, G. C. *Polymer* **2006**, *47*, 4789.

65. Regev, O.; Vandebril, S.; Zussman, E. *Polymer* **2010**, *51*, 2611.

66. Richard-Lacroix, M.; Pellerin, C. *Macromolecules* **2013**, *46*, 9473.

67. Buttaro, L. M.; Drufva, E.; Frey, M. W. *J. Appl. Polym. Sci.* **2014**, *131*, DOI: 10.1002/app.41030.